Journal of The Electrochemical Society, **153** (5) D85-D90 (2006)
0013-4651/2006/153(5)/D85/6/$20.00 © The Electrochemical Society

Model of Multiple Metal Electrodeposition in Porous Electrodes

D. Pilone[a] and G. H. Kelsall*,z

Department of Chemical Engineering, Imperial College London, London SW7 2AZ, United Kingdom

An electrochemical process is being developed for recovering metals from shredded waste electrical and electronic equipment by leaching and electrowinning. In a membrane-divided electrochemical reactor, chlorine is generated at the anode and used as oxidant in an external leach reactor, in which the metals are dissolved in an acidic chloride solution. As the resulting metal ion concentrations are relatively low, a porous (e.g., graphite felt) cathode with a large specific surface area and high mass-transport rates is required to achieve acceptable rates and efficiencies of electrodeposition, the counter reaction to the anodic evolution of chlorine. Hence, as a design tool, a mathematical model was developed to predict potential, concentration, current density, and current efficiency distributions for individual metals within the (flow-through) porous cathode, as well as cell voltages and specific electrical energy consumptions of the electrochemical reactor as functions of cathode feeder potential, cathode thickness, porosity, concentrations, and flow rate and direction. To maximize current efficiencies and productivities of the predominant metal, copper, simulations suggest using an initial cathodic feeder electrode potential of −0.5 V (standard hydrogen electrode) to metallize the felt, followed by electrodeposition of the bulk of the metal at −0.3 V (standard hydrogen electrode), optimal felt thicknesses depending on reactant concentrations.
 [DOI: 10.1149/1.2178607]

Manuscript submitted August 29, 2005; revised manuscript received December 23, 2005. Available electronically March 9, 2006.

An electrohydrometallurgical process[1] is being developed for recovering metals such as Ag, Au, Cu, Pd, Pb, and Sn from the increasing volume of waste electric and electronic equipment (WEEE). Such a process involves coupled leaching and electrowinning operations: chlorine produced at a Ti/RuO_2 anode in an acidic chloride solution, as a counter reaction for metal deposition, is used to promote the oxidative dissolution of metals contained in the electronic scrap. Results[2] of leaching experiments on (<8 mm) shredded WEEE in highly concentrated aqueous HCl + NaCl solutions containing electrogenerated chlorine demonstrated essential complete nonselective metal extraction after ca. 6–7 h.[2] With the electrochemical and leaching reactors coupled, to recover the dissolved metals continuously, the resulting metal concentrations are low. Thus, a porous (e.g., graphite felt) cathode with a large specific surface area and high mass-transport rate is required to achieve acceptable rates and current efficiencies of electrodeposition.

As their physical structure enables high space–time yields even at low reactant concentrations, porous electrodes have found many applications. The theory behind such electrodes has been studied extensively[3,4]and several models have been developed to simulate the behavior of such complex systems.[5-9] Metal electrowinning at flow-through electrodes has been studied for relatively noble metals and for non-noble metals, considering the simultaneous evolution of hydrogen gas bubbles[10,11] that can lead to decreased effective electrolyte conductivity; the model[10,11] treats the effect of gas bubbles on the distribution of potential and coulombic efficiency.

In general, the reaction rate is not uniformly distributed within the electrode because the electrode–electrolyte potential difference, which represents the driving force for the reaction, changes along the electrode depth. This phenomenon is due to ohmic losses within the porous electrode; maximizing the equivalent conductivity is of crucial importance to optimize the effectiveness of three-dimensional electrodes.[12] Porosity has been found to be one of the most important factors determining both solution and electrode phase potentials.

Although the nonuniform potential distribution within the electrode can produce a partial utilization of its internal area, it can enable selective recovery of metals from solutions containing multiple dissolved metals. A theoretical model available in the literature shows the degree of separation of two or more metals as a function of applied potential and solution flow rates.[13,14] This model has been developed assuming isothermal conditions, that the electrode phase is an isopotential surface, and that in the case of metal deposition in the presence of a redox couple, electrodeposition proceeds independently of the redox reaction.

The objective of the work reported in this paper was to predict the effects of the main experimental variables on potential, partial current, and current efficiency distributions. The mathematical model was developed as a tool to design the electrowinning cell and to select the optimal process parameter values.

Mathematical Model

Figure 1 shows a schematic of the membrane-divided reactor with a porous cathode, Ti/RuO_2 anode, and reference electrode; directions of electrolyte and current flows are also shown. Since the electrolyte is a multiple-metal solution containing dissolved Au, Cu, and Fe, the following reduction reactions have been considered

$$AuCl_4^- + 2e^- \rightarrow AuCl_2^- + 2Cl^- \quad [1]$$

$$AuCl_2^- + e^- \rightarrow Au + 2Cl^- \quad [2]$$

$$Cu^{2+} + 2Cl^- + e^- \rightarrow CuCl_2^- \quad [3]$$

$$CuCl_2^- + e^- \rightarrow Cu + 2Cl^- \quad [4]$$

$$FeCl_2^+ + e^- \rightarrow Fe^{2+} + 2Cl^- \quad [5]$$

$$Fe^{2+} + 2e^- \rightarrow Fe \quad [6]$$

Probable side reactions are hydrogen evolution and reduction of chlorine

$$2H^+ + 2e^- \rightarrow H_2 \quad [7]$$

$$Cl_2 + 2e^- \rightarrow 2Cl^- \quad [8]$$

The rate of reaction (Eq. 8) needs to be minimized by depleting the dissolved chlorine in the leach reactor, minimizing its concentration in the electrolyte fed to the cathode, which would cause losses in current efficiencies for metal deposition.

The one-dimensional model, which treats the porous electrode as a superimposition of two continuous phases, was developed with the following assumptions: (*i*) porosity and specific surface area of the cathode were constant; (*ii*) axial dispersion was negligible; and (*iii*) the electrowinning reactor operated under isothermal conditions.

The extended Butler–Volmer equation was used to describe the kinetics of metal ion and chlorine reduction and Tafel's equation was used for hydrogen evolution, using judiciously chosen kinetic parameters.[15] This involved simplification of the complex reduction mechanism of, e.g., Au(III) in chloride media. The local overpoten-

[a] Permanent address: Dip. ICMMPM, Università di Roma "La Sapienza," 00184 Roma, Italy.
* Electrochemical Society Active Member.
z E-mail: g.kelsall@imperial.ac.uk

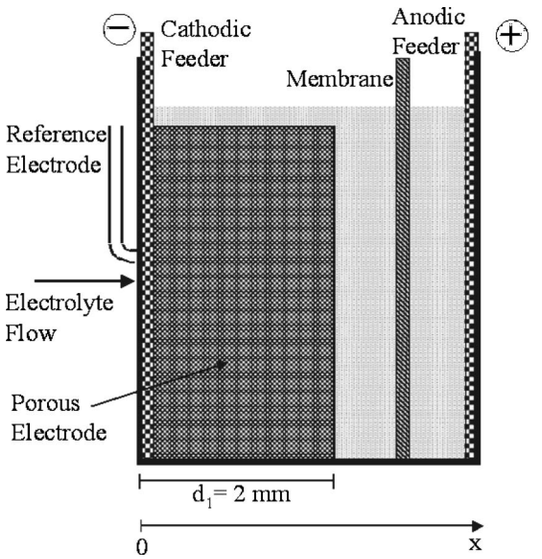

Figure 1. Schematic of membrane-divided reactor with porous cathode and Ti/RuO_2 anode.

tial η_i for each reduction reaction can be expressed as a function of electrode potential ϕ_e, electrolyte potential ϕ_s, and equilibrium electrode potential E_i

$$\eta_i = \phi_e - \phi_s - E_i \quad [9]$$

Applying Ohm's law to the solution and electrode phases results in the following second-order differential equations, relating the local current densities $j(x)$, solution potentials $\phi_s(x)$, and electrode phase potentials $\phi_e(x)$

$$\frac{d^2\phi_s}{dx^2} = -A_s\frac{j(x)}{\sigma_s} \quad [10]$$

$$\frac{d^2\phi_e}{dx^2} = A_s\frac{j(x)}{\sigma_s} \quad [11]$$

where A_s is the electrode specific surface area, and σ_s and σ_e are the effective conductivities of the electrolyte and electrode, respectively, defined by[16]

$$\sigma_s = \sigma_{s0}(\epsilon)^{1.5} \quad [12]$$

$$\sigma_e = \sigma_{e0}(1-\epsilon)^{1.5} \quad [13]$$

The local current density was assumed to be the algebraic sum of the individual currents due to the reduction of each species i, i.e., interactions were neglected in the first instance

$$j(x) = \sum_i j_i(x) \quad [14]$$

The local limiting current density $j_{Li}(x)$, due to the reduction of each species i, is related to the local mass-transfer coefficient k_m and to the bulk concentration $c_i(x)$ by

$$j_{Li}(x) = nFk_m c_i(x) \quad [15]$$

k_m can be calculated from[17]

$$k_m = 3.19\left(\frac{D}{d_h}\right)\left(\frac{v_{eff}d_h}{\mu}\right)^{0.69} \quad [16]$$

in which the solution velocity in the empty cross section of the felt may be calculated as $v_{eff} = v/\varepsilon$ and the hydraulic diameter of the felt fibers as $d_h = d\varepsilon/(1-\varepsilon)$. Among several empirical correlations available in the literature, obtained for different porous electrodes, correlation Eq. 16 appeared the most appropriate, as it was derived from experimental data for a carbon felt electrode.

The mass balances for each reduced species i relate the local concentrations $c_i(x)$ to the local reaction current densities at electrolyte velocity v

$$vnF\frac{dc_i(x)}{dx} = A_s j_i(x) \quad [17]$$

A system of nine differential equations (7, mass balances of Eq. 17 and Eq. 10 and 11) describes the distributions in the porous electrode of nine parameters, i.e., $c_i(x)$, $\phi_s(x)$, and $\phi_e(x)$. The boundary conditions are

$$x = 0 \quad c_i(x) = c_{in} \quad [18]$$

$$x = 0 \quad \frac{d\phi_s(x)}{dx} = 0 \quad \phi_s(x) = 0 \quad \phi_e(x) = P_c \quad [19]$$

$$x = d_1 \quad \frac{d\phi_s(x)}{dx} = 0 \quad [20]$$

where c_{in} is the inlet concentration of each species i and P_c is the cathode feeder potential.

In the model, the reduction of Cu(II) to metallic copper has been treated considering the following simplified reaction mechanism, in which the subscript s implies species at the electrode surface

$$Cu^{2+} \underset{k_m}{\overset{k_m}{\leftrightarrows}} Cu^{2+}_{(s)} \quad [21]$$

$$Cu^{2+}_{(s)} + 2Cl^- + e^- \xrightarrow{k_{cl}} CuCl^-_{2(s)} \quad [22]$$

$$CuCl^-_{2(s)} \underset{k_m}{\overset{k_m}{\rightleftarrows}} CuCl^-_2 \quad [23]$$

$$CuCl^-_{2(s)} + e^- \xrightarrow{k_{c2}} Cu + 2Cl^- \quad [24]$$

From a steady-state mass balance on $Cu^{2+}_{(s)}$, $(d[Cu^{2+}]_s/dt = 0)$, and $CuCl^-_{2(s)}$, $(d[CuCl^-_2]_s/dt = 0)$

$$k_m[Cu^{2+}] - k_m[Cu^{2+}]_s - k_{cl}[Cu^{2+}]_s = 0 \quad [25]$$

$$k_{cl}[Cu^{2+}]_s - k_{c2}[CuCl^-_2]_s - k_m[CuCl^-_2]_s + k_m[CuCl^-_2] = 0 \quad [26]$$

The current densities due to the reduction of Cu(II) to Cu(I) and of Cu(I) to metallic copper are, respectively, given by

$$j_{Cu(II)} = -Fk_{c1}[Cu^{2+}]_s \quad j_{Cu(I)} = -Fk_{c2}[CuCl^-_2]_s \quad [27]$$

where

$$k_{ci} = k_{i,0}\exp\left\{\frac{-\alpha_i F\eta}{RT}\right\} \quad [28]$$

The mass balance for Cu(II) is given by Eq. 17, while the following equation

$$vnF\frac{d[CuCl^-_2]}{dx} = A_s(J_{Cu(I)} - j_{Cu(II)}) \quad [29]$$

represents the Cu(I) mass balance. In the code, the analogous reduction mechanism (Reactions 21-24) used for Cu(II) was adopted for the reduction of Fe(III).

Numerical solutions of the differential equation system were found using Maple's 'dsolve'/numerical boundary value problem solver.[18]

Results and Discussion

The formulated mathematical model enables computation of the distributions of overpotentials, partial current densities, and metal ion concentrations within the porous electrode. The results reported

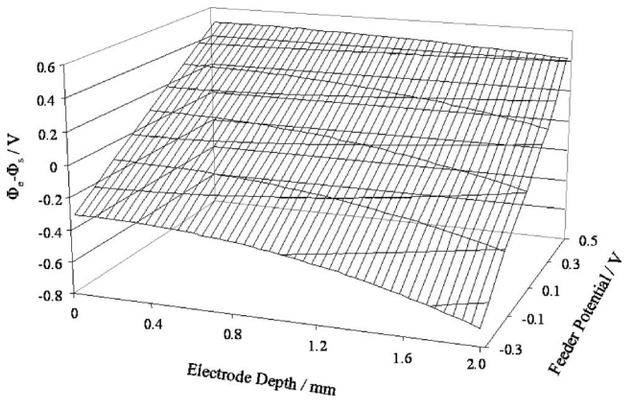

Figure 2. Effects of feeder electrode potential and electrode depth on the difference between metallized graphite electrode and solution phase potentials.

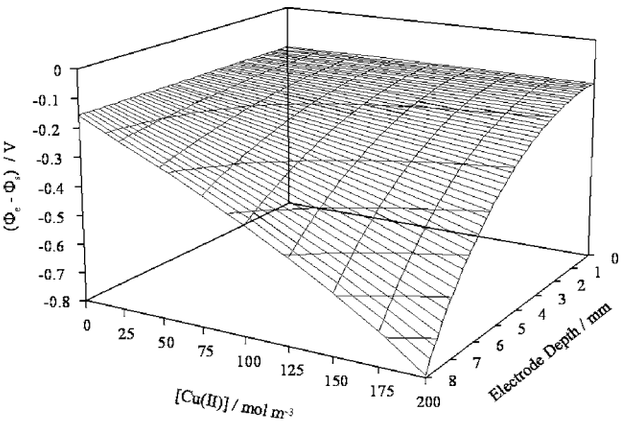

Figure 3. Effects of Cu(II) reactant concentration and electrode depth in the direction of current flow on the difference between metallized graphite electrode and solution phase potentials.

here are for graphite felt electrodes, having a specific surface area equal to 5000 m^{-1} and a porosity of 0.95. The results reported in a previous paper[19] showed that in an uncoated graphite electrode, the driving force for the reduction reactions is higher close to the cathodic feeder, where reduction reactions occur preferentially.

Although the published results[19] enable prediction of potential and partial current distributions within the uncoated carbon felt electrode, as soon as a metallic layer is deposited on the electrode surface the resistivity increases greatly, changing the electrode behavior. The calculation of electrode resistance as a function of metal coating thickness shows that the resistance switches between that of carbon and that of copper, which is the main component of the deposited alloy, even for 100-nm-thick deposits. In order to choose the optimal operating conditions and reactor geometry, it is of crucial importance to predict the behavior of metallized carbon felt electrodes. Hence, several simulations were performed to predict their behavior assuming an electrode phase bulk conductivity of 5.9×10^7 S m^{-1}. The electrolyte composition considered in the numerical simulation was that from leaching of shredded WEEE with a solid/liquid ratio equal to 1:5. The concentrations of the more important elements were 472 mol m^{-3} Cu, 268 mol m^{-3} Fe, and 0.1 mol m^{-3} Au. Other elements present in the real electrolyte have been neglected, since the system considered is already rather complex; their inclusion results in greatly increased computation times. However, as the concentration of other elements in the real leach solutions is low, their reduction reactions do not significantly affect potential and current distributions within the porous electrode. After predicting potential distribution, the different areas/volumes where such elements are preferentially reduced can be determined easily.

The results showed that whatever the applied potential, the electrode-solution potential difference in the porous electrode increases with distance from the feeder electrode (Fig. 2). In the proposed process, possible side reactions are hydrogen evolution by Reaction 7 and reduction of chlorine by Reaction 8; to avoid losses in current efficiencies the rate of Reaction 8 can be minimized by depleting the dissolved chlorine before the solution is fed in the cathodic compartment. The rate of hydrogen evolution needs to be constrained by judicious selection of reactor operating parameter values and geometry. At the more negative potentials, the simulations suggest the use of an electrode no thicker than 2 mm, as used in all subsequent simulations. The optimal thickness of the electrode depends on reactant concentrations: as Cu(II) ions predominate in the leach solution, from which many metals are to be recovered, the behavior of Cu(II) determines local current density distributions, the potential profile along the porous electrode, and the behavior of other species. Figure 3 shows that the increasing driving force along the electrode becomes more pronounced with increasing Cu(II) reactant concentration, as a consequence of the increased partial current densities due to the reduction of Cu(II) to Cu(I), then Cu^0. At the high concentrations (472 mol m^{-3}) used in the simulations, for electrodes thicker than 2 mm in the direction of current and electrolyte flow, hydrogen evolution decreased current efficiencies drastically and made the cell inoperable due to gas bubbles filling the voidage in the felt.

Figure 4 shows the Cu(I) concentration to increase with the distance from the feeder electrode and with decreasing feeder electrode potential from 0.5 V [standard electrode potential (SHE)], the rate of Reaction 22 increasing. However, the Cu(I) concentration passes through a maximum at 0.1 V (SHE) and decreases at lower potentials due to further reduction of Cu(I) ions to copper occurring by Reaction 24 causing Cu(I) depletion.

The local partial current density distribution (Fig. 5) for the reduction of Cu(I) to metallic copper shows that copper deposition does not occur at feeder electrode potentials $\geqslant 0.1$ V (SHE). At -0.1 V (SHE), copper deposits in the volume of the cathode furthest from the feeder electrode; this is due to the reaction overpotential increasing with distance from the feeder electrode and reaching a maximum value of -0.6 V when $x = 2$ mm. At feeder electrode potentials < -0.1 V (SHE), the current density profiles are affected both by the overpotential, which increases with distance from the feeder, and the concentration of Cu(I) formed by Reaction 22. Figure 6 shows the effects of both electrode depth and applied potential on overall current efficiency for metal deposition, calculated considering hydrogen evolution and chlorine and Fe(III) reduction as parasitic reactions. For the operating conditions considered, Fe(III) can

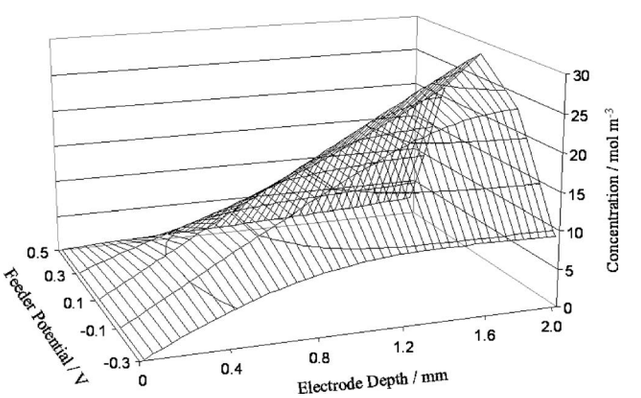

Figure 4. Effects of feeder electrode potential and electrode depth on Cu(I) concentration in the bulk solution with metallized graphite felt.

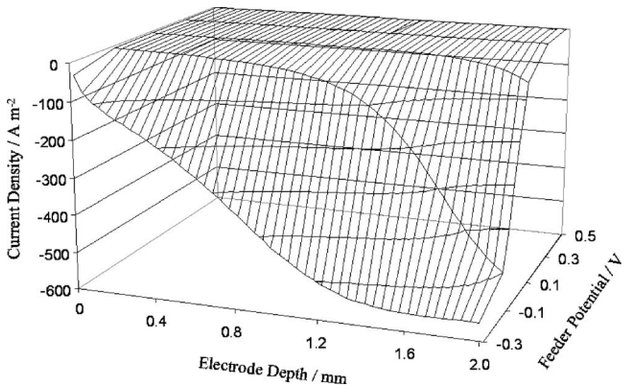

Figure 5. Effects of feeder electrode potential and electrode depth on partial current density for reduction of Cu(I) to Cu metal.

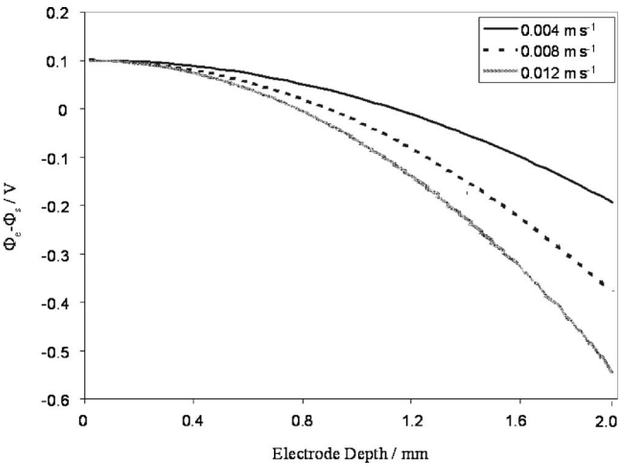

Figure 7. Effects of electrolyte velocity and electrode depth on the difference between metallized graphite electrode and solution phase potentials, with an applied feeder potential of 0.1 V (SHE).

be reduced via Fe(II) to metallic iron only to a very limited extent, even at the most negative applied potentials; hence, from a recovery process perspective, the charge passed for Fe(III) reduction can be considered wasted. As shown in Fig. 6, current efficiencies were predicted as $<75\%$, reaching values of about 20% at the more positive potentials, at which most of the charge passed is used for the reduction of Fe(III) to Fe(II). At a feeder electrode potential of -0.3 V (SHE), hydrogen evolution resulted in the sharp decrease of current efficiency furthest from the feeder. In the envisaged process conditions, iron(II) would accumulate in the solution. This could be minimized either by subjecting the shredded WEEE to more selective mechanical pretreatment and magnetic separation and/or bleeding a portion of the solution periodically from the flow circuit and using another electrochemical reactor, with conditions optimized for iron deposition, at higher temperatures and higher pH.

As shown in Fig. 7, increasing electrolyte velocity increased the range of potentials in the electrode for a feeder potential of 0.1 V (SHE) by enhancing mass-transport rates and hence increasing current densities. As the overpotential distribution within the electrode determines current efficiencies, when the electrode potential is <-0.5 V (SHE), the sharp increase of current density due to the reduction of Cu(I) to metallic copper enhances current efficiencies, which, as shown in Fig. 8, reach a value of about 77% in the electrode area/volume furthest from the feeder electrode.

As the electrodeposition proceeds, the electrode becomes less and less porous, with consequential changes in current and potential distributions. Figure 9 predicts that electrode-solution potential differences increase as effective electrolyte conductivities diminish with decreasing porosity. As mentioned above, knowledge of the distribution of hydrogen overpotential, which increases with increasing electrode depth and with decreasing porosity, is of critical importance in defining the optimal reactor design and operating conditions. Figure 10 predicts that the distribution of H_2 evolution partial current density in the porous electrode could result in the reactor becoming inoperable with increasing electrodeposition time and decreasing cathode porosity, due to the sharp increase of hydrogen evolution furthest from the feeder electrode.

The predictions in Fig. 2-10 were obtained with the model's electrolyte flowing in the positive x axis direction, as shown in Fig. 1. When the electrolyte flow was reversed, Fig. 11 predicts lower ranges of potential differences between solution and electrode phases as a function of electrode depth (x). In fact, Cu(II) and Fe(III) concentrations were then lower close to the feeder electrode, where the driving force is lower, producing an overall decrease in current density. Reversing the electrolyte flow direction causes different concentration profiles in solution and, hence, different electrowon alloy compositions as a function of electrode depth. Figure 12 shows that copper is predicted to be more homogenously distributed along the electrode when the flow is reversed, because the Cu(I) concentration in the electrolyte increased toward the feeder electrode, favoring copper deposition in that area/volume.

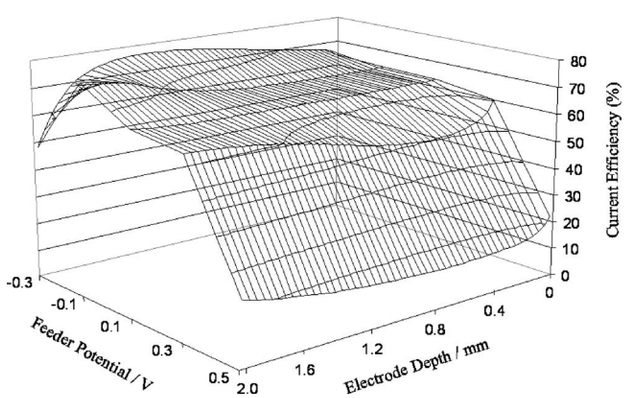

Figure 6. Effects of feeder electrode potential and electrode depth on current efficiency.

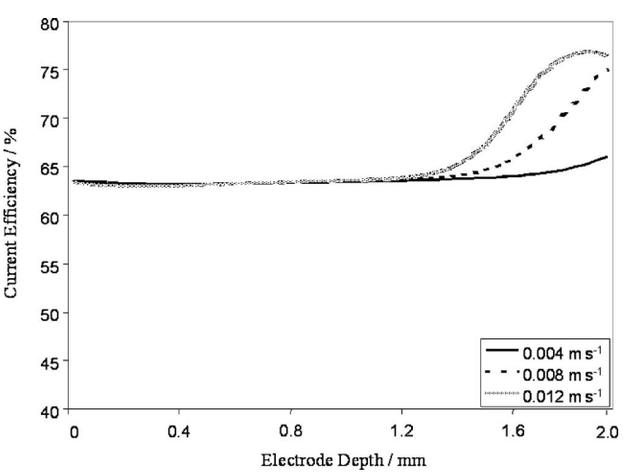

Figure 8. Effects of electrolyte velocity and electrode depth on current efficiency, with an applied feeder potential of 0.1 V (SHE).

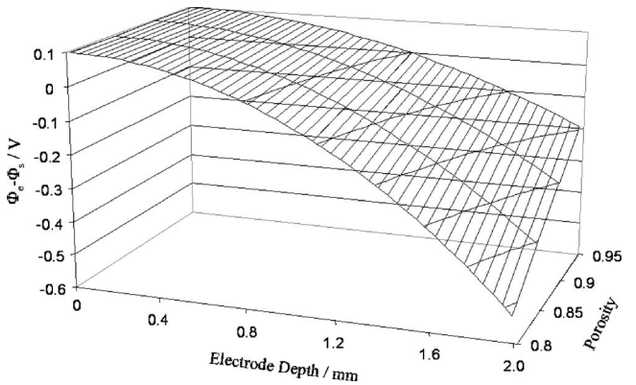

Figure 9. Effects of electrode porosity and electrode depth on the difference between metallized graphite electrode and solution phase potentials.

The results predicted that once the electrode had been metallized, the effective electrode conductivity (ca.. 66×10^4 S m^{-1}) increased little, whereas the effective solution conductivity (initially ca. 60 S m^{-1}) decreased as deposition occurred due to the decreased voidage, causing increasing overpotentials furthest from the feeder electrode. With electrode conductivity orders of magnitude greater than that of the electrolyte, it would be preferable either to use low reactant concentrations, as implied by results in Fig. 3, or to use several thin electrodes in reactors in series, in order to constrain the range of overpotentials in each one and hence obtain both high productivities and current efficiencies. Electrodepositing metal ions at −0.3 V (SHE) while feeding the electrolyte to the cathodic compartment from the feeder side appeared to be the most advantageous choice of conditions, because it improved the degree of separation of different metals during electrodeposition and limited the rate of hydrogen evolution.

Conclusions

The mathematical model developed enables simulation of electrodeposition of multiple metals at porous electrodes, by computation of spatial distributions of overpotentials, partial current densities, and concentrations, which is essential to the design of such electrochemical reactors and to selecting their optimal operating conditions. As copper and iron ions predominate in the leach solution from which a range of metals are to be recovered, the behavior of Cu(II) and Fe(III) determines the electrode potential distribution and hence the behavior of other solution species. Selection of felt thickness and of operating conditions to limit current efficiency losses depend on the distribution of hydrogen partial current densities. Once the felt becomes metallized, increasing its effective conductivity to four orders of magnitude greater than that of the electrolyte, overpotentials and current densities are then highest in that volume of the felt furthest from the feeder and closest to the counter electrode. To minimize the rate of hydrogen evolution in that volume and maximize overall current efficiency and productivities, simulations suggested using a cathode feeder electrode potential of −0.3 V (SHE) for the electrodeposition of the bulk of the metal. Even so, to obtain acceptable current efficiencies, felt thicknesses of ca. 2 mm in the direction of current and electrolyte flow were required at the concentrations notionally used in the simulations. Hence, to achieve high conversions in a single pass, several such thin electrodes in series would be required. Simulations suggest also that cathodes have to be replaced frequently; as porosities decrease with increasing electrodeposition time, drastic changes in overpotential distributions can occur, promoting H_2 evolution furthest from the feeder. Evidently, for high reactant concentrations, a consolidated porous cathode, such as a felt, is an inappropriate design for metal electrodeposition.

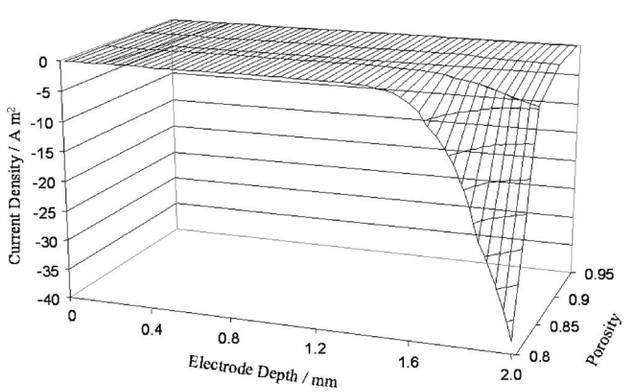

Figure 10. Effects of electrode porosity and electrode depth on partial current density for H_2 evolution at metallized graphite felt, with an applied feeder potential of 0.1 V (SHE).

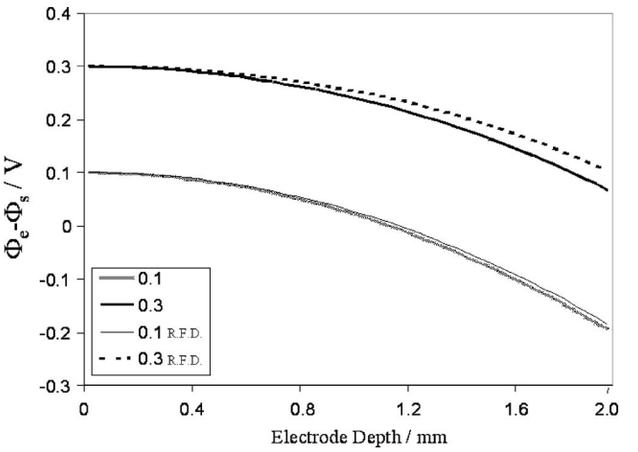

Figure 11. Effects of electrolyte flow direction and electrode depth on the difference between metallized graphite electrode and solution phase potentials, with an applied feeder potential of 0.1 and 0.3 V (SHE). R.F.D. indicates the results obtained when the electrolyte flow is reversed.

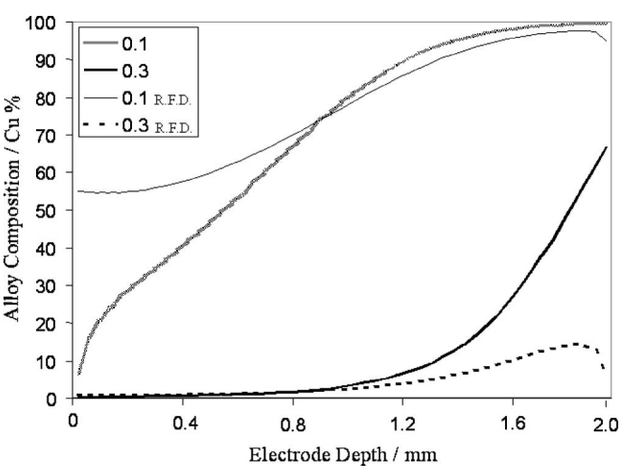

Figure 12. Effects of electrolyte flow direction and electrode depth on the copper content of the electrowon alloy, with an applied feeder potential of 0.1 and 0.3 V (SHE). R.F.D. indicates the results obtained when the electrolyte flow is reversed.

Acknowledgements

G.H.K. thanks the UK Engineering and Physical Sciences Research Council (EPSRC) for a grant. D.P. thanks Università di Roma "La Sapienza" for granting her a year's leave of absence at Imperial College London.

List of Symbols

A_s	electrode specific surface area, m^{-1}
c_i	electrolyte concentration of species i, mol m^{-3}
D	pore diameter of electrode, m
d_h	hydraulic diameter of the felt fibers, m
d_1	electrode thickness in direction of current flow, m
d	diffusion coefficient, m^2 s^{-1}
E_i	equilibrium electrode potential vs reference electrode, V
F	Faraday constant, 96,485, C mol^{-1}
j	local current density, A m^{-2}
j_i	local current density for the reduction of species i, A m^{-2}
j_L	local mass-transport-controlled current density, A m^{-2}
j_{Li}	local mass-transport-controlled current density for the reduction of species i, A m^{-2}
k_m	mass transport rate coefficient, m s^{-1}
k_{ci}	potential-dependent rate coefficient for Reactions 21 and 24, s^{-1}
$k_{i,0}$	standard rate coefficient according to Eq. 28, m s^{-1}
N	charge number of reaction, 1
P_c	cathode feeder potential, V
R	gas constant, 8.31441, J mol^{-1} K^{-1}
t	time, s
T	absolute temperature, K
v	electrolyte velocity, m s^{-1}
v_{eff}	solution velocity in the empty cross section, m s^{-1}

Greek

α	transfer coefficient for reaction, 1
ε	electrode porosity, 1
ϕ_e	electrode potential, V
ϕ_s	solution potential, V
σ_{e0}	electrode specific conductivity, S m^{-1}
σ_{s0}	electrolyte specific conductivity, S m^{-1}
σ_e	effective electrode conductivity, S m^{-1}
σ_s	effective electrolyte conductivity, S m^{-1}
η_i	local overpotential for the reduction of species i, V
μ	electrolyte kinematic viscosity, m^2 s^{-1}

References

1. N. P. Brandon, G. H. Kelsall, T. Müller, R. Olijve, M. Schmidt, and Q. Yin, in *Energy and Electrochemical Processes for a Cleaner Environment*, C. Comninellis, M. Doyle, and J. Winnick, Editors, PV 2001-23, pp. 323–338, The Electrochemical Society Proceedings Series, Pennington, NJ (2001).
2. N. P. Brandon, G. H. Kelsall, M. J. Schmidt, and Q. Yin, in *Recycling and Waste Treatment in Mineral and Metal Processing: Technical and Economic Aspects*, B. Björkman, C. Samuelsson, and J-O. Wilkström, Editors, pp. 359–368, TMS, Warrendale, PA (2002).
3. J. Newman and W. Tiedman, in *Advances in Electrochemistry and Electrochemical Engineering*, Vol. 11, H. Gerischer and C. W. Tobias, Editors, p. 353–438, Interscience/Wiley, New York (1978).
4. J. S. Newman and C. W. Tobias, *J. Electrochem. Soc.*, **109**, 1183 (1962).
5. J. M. Bisang, K. Juttner, and G. Kreysa, *Electrochim. Acta*, **39**, 1297 (1994).
6. G. Kreysa, *Electrochim. Acta*, **23**, 1351 (1978).
7. T. Doherty, J. G. Sunderland, E. P. L. Roberts, and D. J. Pickett, *Electrochim. Acta*, **41**, 519 (1996).
8. Y. Sun and K. Scott, *Chem. Eng. J. (Lausanne)*, **102**, 83 (2004).
9. A. I. Masliy and N. P. Poddubny, *J. Appl. Electrochem.*, **27**, 1036 (1997).
10. M. M. Saleh, J. W. Weidner, and B. G. Ateya, *J. Electrochem. Soc.*, **142**, 4113 (1995).
11. M. M. Saleh, *J. Phys. Chem. B*, **108**, 13419 (2004).
12. Y. Volkman, *Electrochim. Acta*, **24**, 1145 (1979).
13. R. C. Alkire and R. M. Gould, *J. Electrochem. Soc.*, **123**, 1842 (1976).
14. R. M. Gould and R. C. Alkire, *J. Electrochem. Soc.*, **126**, 2125 (1979).
15. D. Pilone and G. H. Kelsall, *Electrochim. Acta*, (2006) In press.
16. R. E. Meredith and C. W. Tobias, in *Advances in Electrochemistry and Electrochemical Engineering*, Vol. 2, P. Delahay and C. W. Tobias, Editors, p. 15, Interscience/Wiley, New York (1962).
17. R. Carta, S. Palmas, A. M. Polcaro, and G. Tola, *J. Appl. Electrochem.*, **21**, 793 (1991).
18. www.maplesoft.com
19. D. Pilone and G. H. Kelsall, in *Electrochemistry in Mineral and Metal Processing VI*, F. M. Doyle, G. H. Kelsall, and R. Woods, Editors, PV 2003-18, p. 260, The Electrochemical Society Proceedings Series, Pennington, NJ (2003).